Random interfaces generated by the addition of structures of variable size

Nicolas Pétrélis, François Pétrélis

Random interfaces generated by the addition of structures of variable size

Nicolas Pétrélis
Laboratoire Jean Leray, Université de Nantes, 2, rue de la Houssinière, 44322 Nantes Cedex 3, France

François Pétrélis
Laboratoire de Physique de l'Ecole normale supérieure, ENS, Université PSL, CNRS, Sorbonne Université, Université Paris-Diderot - Paris, France
(Dated: November 6, 2024)

We consider the random deposition of objects of variable width and height over a line. The successive additions of these structures create a random interface. We focus on the regime of heavy tailed distributions of the structure width. When the structure center is chosen at random, the problem is exactly solvable and the interface generically tends towards a self-affine random curve. The asymptotic behavior reached after a large number of iterations is universal in the sense that it depends on only three parameters: the shape of the added structure at its maximum, the power-law exponent of the width distribution and the exponent that relates height and width. The parameter space displays several transitions that separate different asymptotic behaviors. In particular for a set of parameters, the interface tends towards a fractional Brownian motion. Our results reveal the existence of a new class of random interfaces which properties appear to be robust. The mechanism that generates correlations at large distance is identified and it explains the appearance of such correlations in several situations of interest such as the physics of earthquakes or the propagation of energy through a diffusive medium.

The evolution of an interface that is modified by the successive addition of objects is an iconic problem of statistical physics with applications ranging from the deposit of a granular [1] to the growth of a stable phase into a metastable one or to the propagation of a flame to quote but a few [2]. In the past decades, the competition between randomness and diffusion was shown to be modelled by the Edwards-Wilkinson (EW) equation and, when nonlinearity is taken into account, by the Kardar-Parisi-Zhang (KPZ) equation [3]. The quest for their understandings drove a variety of efforts both on the theoretical front [4] or the experimental one [5]. The additive term in these equations is a Gaussian white noise both in time and space and is thus uncorrelated. In a one dimensional geometry, the solutions tend at long time towards a Brownian motion [2]. Gaussian correlated noise has also been considered [6].

There are very few studies that consider the case of the random addition of objects of varying size and they are restricted to either a binary size distribution [7] or a Poisson one [8]. Here, we consider objects that have an heavily tailed distribution of size and show that such a process leads to a new class of random interfaces displaying a variety of behavior. Notably, spatial correlations at large distance appear even when the individual steps of the process are uncorrelated.

The initial motivation for this problem comes from the physics of earthquakes (EQ) [9]. We will thus describe the models in this context. However, the addition of objects of variable size is a quite general situation and applications in the context of interaction of a wave with a diffusive medium will be given at the end of this article.

We have shown in several models that the statistical properties of the EQ result from the stress field being a self-affine random curve [9]. More precisely, in a 1D geometry, the large scales of the stress field tend towards a Brownian motion or a fractional Brownian motion (fBm). This property originates in the stress field evolution that results from the successive stress changes caused by the EQ. The mechanism is the following iterative sequence: the stress field at a given time controls the properties of the next EQ and in particular the amount of slip caused by the event; the slip is in turn responsible for the modification of the stress. After a large number of iterations, this process builds up a self-affine stress field. We identified this process in several models and showed that it is responsible for the intriguing properties of EQ [9, 10], such as the distribution of the released energy (the Gutenberg-Richter law) or the distribution of aftershocks after a main shock (the Omori law). It is thus expected that this process is generic, robust and can be observed in idealized models of EQ. Nevertheless, the origin of the large distance correlations, as displayed by the self-affine stress field, is unclear. The purpose of this article is to identify why and when such large distance correlations appear. To achieve this goal, we consider two models, solve rigorously one of them and study them numerically.

The simplest model of evolution of a stress field is to consider that it is a scalar function of space and that successive EQ change its value. Between events, the stress increases due to tectonic loading and this is usually considered as a spatially uniform linear in time increase of the stress. When the stress reaches a threshold, an EQ is initiated. After the event, the stress in the domain that has moved is decreased.

In order to deal with positive quantities, we define $h(x)$ as the opposite of the stress and assume that each event results in the addition of a value $\delta h(x)$ to $h(x)$. The

linear in time loading between events is not considered here as it only amounts to a change in the spatial average of h. The problem is thus turned into the evolution of an interface $h(x)$ that drifts towards positive values because of the successive deposition of objects that change its value by a quantity $\delta h(x)$.

An EQ affects the fault property over a size which is distributed as a power-law [9, 12] and we thus assume that δh is non zero over a width similarly distributed.

We consider two variations of this process. Earthquakes are usually initiated at locations at which the stress is maximum, which corresponds to the minimum value of h: this is the min-model. We also consider a simpler situation, the rand-model in which the stress drop or equivalently the change of h occurs at a random position, independent of the value of h.

In a more formal way, we consider positions on a line $x \in [0, D]$. We use periodic boundary conditions to maintain homogeneity in the statistical properties of the system. We are interested in $h_N(x)$ the height after N iterations. An iteration consists in the addition of $\delta h(x)$ defined as follows. Let $\psi : [0, 1] \mapsto \mathbb{R}^+$ be a continuous function, such that $\psi(0) = 1$ and $\psi(1) = 0$, and let n be the index of its first non zero derivative at 0^+. For $n = 1$, ψ is locally a triangle, for $n = 2$ a parabola... Let s be the center of the structure which is either drawn at random over $[0, D]$ for the rand-model or which is the minimum of $h(x)$ for the min-model. Let U be the width of the structure. It is a random variable distributed as a Pareto law with parameter $\beta-1$ ($\beta > 1$), i.e., with density $1_{[1,\infty)}(u)(\beta-1)/u^\beta$. Let $v_s(x) = \min\{|s-x+jD|, j \in \mathbb{Z}\}$ be the distance between the center and the position x, where we use the periodicity of the system. We then define

$$\delta h(x) = U^{\alpha-1}\ 1_{[0,U[}(v_s(x))\ \psi\Big(\frac{v_s(x)}{U}\Big). \qquad (1)$$

In other words, at each iteration, we add a structure of shape ψ of width $2U$ and of amplitude $U^{\alpha-1}$. The structure is even with respect to its center and its width is random and distributed as a power-law of exponent $-\beta$.

These processes can be simulated numerically and we display in fig. 1 profiles of $h = h_N(x)$ calculated over a grid of spacing $\Delta x = 1$ when ψ is linear so that the added structure is a triangle ($n = 1$).

For both models, several results can be proven rigorously using probabilistic methods applied to random curves. Details are provided in the appendix but we focus here on the results. Interestingly, they depend exclusively on n, α and β.

The spatial average of h increases with N either linearly (ballistic) for $\beta > \alpha$ or as $N^{\frac{\alpha-1}{\beta-1}}$ (super-ballistic) for $\beta < \alpha$. More precise estimates are given in Eq. 8, 9 and 10.

For the rand-model, we are able to fully describe the spatial fluctuations of h. Let $f_N(x) = h_N(x) - h_N(0)$.

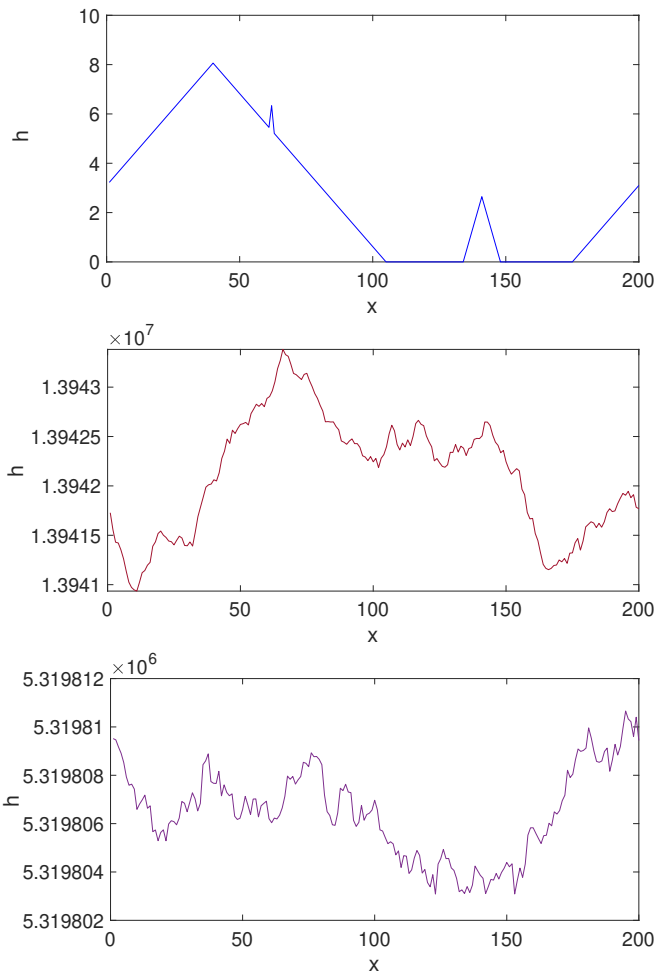

Figure 1. Numerically simulated interface $h(x) = h_N(x)$ for a segment of length $D = 200$, $\alpha = 1.5$ and $\beta = 1.5$. Top: rand-model after $N = 3$ iterations starting from a straight line. Middle: rand-model after $5\,10^5$ iterations. Bottom: min-model after $5\,10^5$ iterations.

1. For $\alpha > 1 + n$ and $1 < \beta \leq \beta_c := 2\alpha - 1 - 2n$

$$N^{-\frac{\alpha-1-n}{\beta-1}} f_N \Rightarrow_N \mu, \qquad (2)$$

where μ is the distribution of a random function which can be expressed as the limit of a sum of random functions, see Eq. 11, 12 and 13. In particular the fluctuations of h are not a Gaussian process.

2. For $\alpha \in [1, 1 + n]$ or for $\alpha > 1 + n$ and $\beta > \beta_c$

$$N^{-\frac{1}{2}} f_N \Rightarrow_N Y, \qquad (3)$$

where Y is a centered Gaussian process.

In this case, we are able to derive an analytical expression for the covariance $r(s,t) = \mathrm{Cov}\,(Y(s), Y(t))$. We verified by estimating the quantities numerically that for $\beta \geq \beta_f := 2\alpha - 2$ and for $D \gg s, t \gg 1$, $r(s,t) \propto |s|^{2H} + |t|^{2H} - |s-t|^{2H}$ with $2H = 2\alpha - \beta$. When $\beta \leq \beta_f$, the covariance is dominated by quadratic terms in s or t.

We draw the parameter space of the rand-model in fig. 2. It contains 3 transitions separating 6 different behaviors.

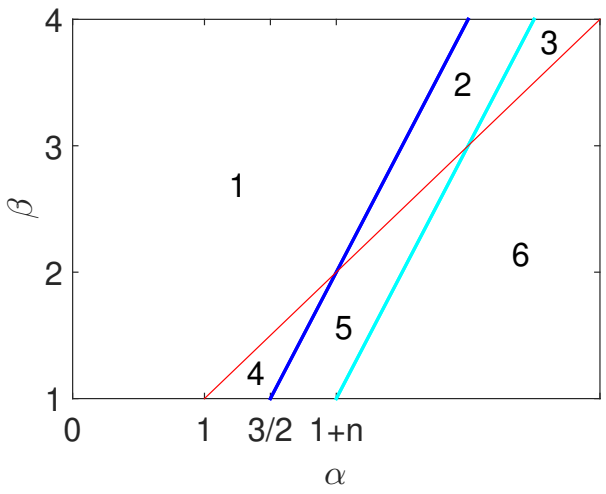

Figure 2. Parameter space describing the behavior of the interface $h_N(x)$ at large N for the rand-model. The red line is $\beta = \alpha$ and separates between a ballistic (domain 1, 2 and 3) and a super-ballistic (4, 5 and 6) behavior of the mean position of the interface. The cyan line is $\beta_c = 2\alpha - 1 - 2n$ and separates between a Gaussian (1, 2, 4, 5) and a non Gaussian (3, 6) behavior of the field fluctuations. The blue line is $\beta_f = 2\alpha - 2$ and separates between a $x^{2\alpha-\beta}$ behavior (1 and 4) of the correlations of the fluctuations and a x^2 one (2, 3, 5, 6).

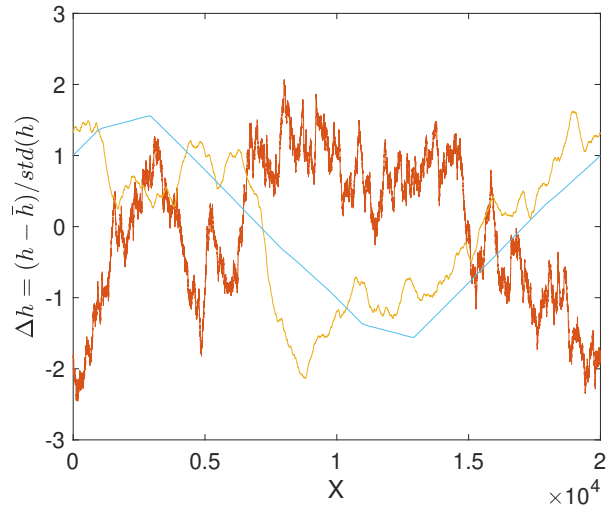

Figure 3. For the rand-model and for $\beta = 2$, normalized height profile as a function of position after $N = 10^7$ iterations for a triangular added structure ($n = 1$) and for (red) $\alpha = 1.5$, (yellow) $\alpha = 2$ and (light blue): $\alpha = 3$.

A particularly interesting regime concerns $0 \leq 2\alpha - \beta \leq 2$. Then the process generates a fBm of Hurst exponent H with

$$H = \alpha - \beta/2\,. \tag{4}$$

The value of the Hurst exponent can be understood as follows. The difference of height $\langle f_N(l)^2 \rangle$ between two sites distant of l is due to events of size L larger than l which center is within a neighborhood of one of the two sites over a width proportional to l. These events provide a height difference of order $l^{\alpha-1}$. When the integral is dominated by the smaller values of L, we obtain the estimate

$$\langle f_N(l)^2 \rangle \simeq l\, l^{2\alpha-2} \int_l^\infty L^{-\beta} dL \simeq l^{2\alpha-\beta}.$$

It is worth noting that this result does not depend on n and is thus independent of the shape of the added structures.

Examples of profiles are presented in fig. 3. We calculate from these profiles the power spectrum density (PSD) of $f_N/N^{1/2}$. The power law of the PSD, K^{-1-2H} for a fBm, allows to calculate H, which is displayed in fig. 4. It verifies the prediction of Eq. (4).

It is worth noting that the phenomenology differs from the one of the KPZ solutions in 1D which tend towards a Brownian motion (with $H = 1/2$) when the noise term is uncorrelated [2] or that transitions between a Brownian motion and a long range correlated regime (with $H > 1/2$) when the noise term is Gaussian and its correlation at long range is increased [6]. Therefore, the models that we present here belong to a different universality class.

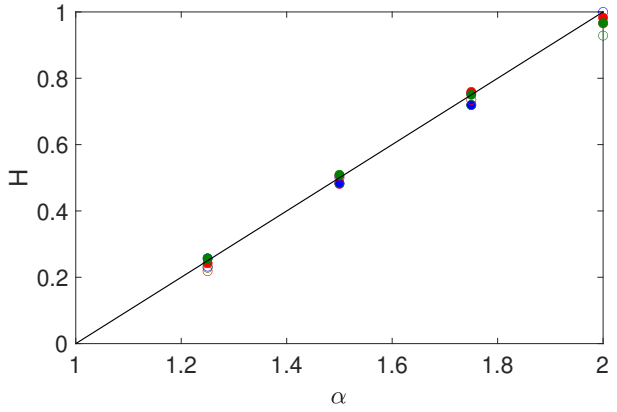

Figure 4. Hurst exponent H as a function of α for $\beta = 2$. The straight line is the prediction $H = \alpha - \beta/2$. Full symbols are results of the rand model and empty symbols of the min model. Red is for $n = 1$ (triangle), blue for $n = 2$ (parabola), green for $n = 2$, parabolic at its center with negative value of δh at its border.

The min-model is a challenging problem for its theoretical aspects as the dynamics relies on a non-local constraint. The results for the spatial average of h are the same as for the rand-model. For the fluctuations we must relate on numerical simulations, see fig. 1 bottom. We

focus here on the regime $0 < 2\alpha - \beta \leq 2$ for which the rand-model generates a fBm. In contrast to the rand-model, the moments of the fluctuations do not increase with N but remain bounded. The skewness is small but non zero, the flatness is slightly smaller than 3, the value for a Gaussian. It increases with the size D. It is quite interesting that the application of the min rule for finding the location of the next earthquake is sufficient to saturate the growth with the number of iterations of the moments of the fluctuations of the stress profile.

The value of H obtained from the PSD is displayed in fig. 4. As for the rand-model, the results are very close to the prediction of Eq. (4). The H-exponent is thus independent of the shape of the added structure and of the nature of the model (rand or min).

In the models considered here, the spatial structure of the stress change is the same at each event, up to a change of its width and height. The shape, the width and the height are independent of h whereas in a fault, it is the spatial variations of h that determine the slip which controls the change of stress. The independence of stress change on the stress (for the rand-model) or of only dependence for its center set by the stress maximum (for the min-model) are simplifications that allow for theoretical progresses. Yet, the observed phenomenology is rich and similar to what is observed in more realistic models [9, 10]. In particular, our results explain why the random addition of structures of variable size generically generates self-affine behavior. In the context of earthquake physics, this phenomenon provides a possible explanation for the appearance of large distance correlations of the stress field.

Several observations in natural data are consistent with our description. It is well known that the earthquake areas are distributed as a power-law with exponent β_a close to 2 [12, 14]. This amount to a distribution of length of the EQ with power-law exponent $\beta \simeq 3$. In addition, the stress change at each event is independent of its length so that α is of order 1 [12]. For what concerns the existence of large scale correlations, the topography of faults are self-affine with their roughness associated to an Hurst exponent of order 0.2 to 0.8 [15]. In addition, evidence suggests that the slip itself scales with a Hurst exponent close to 0.6. Using a 3D fault numerical model it was predicted that the 2D frictional stress field scales with an Hurst exponent of -0.4 [16]. All these fields in nature thus display correlations at large scale.

This new class of random interfaces is of interest for the physics of earthquakes but also as a new stochastic process, different from the ones generated by the EW or the KPZ equation. It has possible applications in a variety of domains. For instance, the deposition of polymers of variable size is expected to belong to this new class provided the polymer size has a wide distribution. Another application of broad interest, which might at first sight appear quite unrelated, is the propagation of a wave through a medium containing objects of variable size. Consider the energy of a plane wave that propagates in a straight line and study its evolution when it interacts with a set of objects that absorb partially the wave energy. When the absorption is proportional to the length of the path of the wave in the object, the wave energy after the object is decreased by a quantity proportional to the width of the object along the path of the wave. This is sketched in fig. 5. The interaction of the wave with a set of absorbers amounts to the sum of the interaction with each one. Therefore the expression for the variation of the wave energy is given by the same formula as the variation of the stress profile in eq. (1). The results obtained here apply identically to the wave energy.

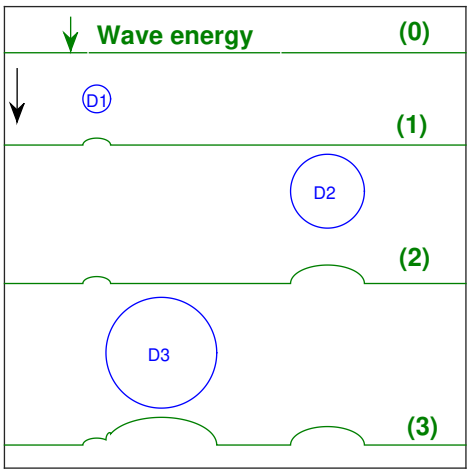

Figure 5. Schematics of the variation of a plane wave that propagates in straight line from the top to the bottom parallel to the black arrow. The wave energy is displayed as a green line. It is decreased at each interaction with an absorbing object D_i sketched as a blue circle and proportionally to the width of the absorber in the direction of propagation. The energy after the (i)-th encounter is displayed for $i = 0$ to 4.

Several applications come to mind. Fragmentation processes often produce collections of object with size distributed as a power-law [18]. This can be the case of drops fragmented in a turbulent flow [19]. An experiment using two fluids matched in index and such that drops of one of the two phases absorb the light at a given frequency would realize the situation of fig. 5 [20]. A second system relies on aerosols in the atmosphere which have a size distribution that can be large [21] and in some situation is modelled by the Junge law [22], a power-law distribution generated by coagulation processes [23]. We expect that the absorption of light or of UV rays through such an aerosol cloud results in energy transmission that varies in the plane perpendicular to the direction of propagation. In the idealized limit where we neglect scattering processes, the energy spatial variation in the perpendicular plane is exactly obtained

by the rand-model. Our results indicate that the pattern of energy should display a self-affine behavior with properties controlled by the distribution of size of the aerosols and it would be interesting to investigate how this is affected when scattering cannot be neglected. Finally, we describe a third example related to the propagation of electromagnetic energy through the universe. Interstellar clouds are domains where the density is large. These clouds are magnetized and their emission at microwave frequencies is polarized. The statistical characterization of this interstellar emission is of prime importance to experiments searching the signature of primordial gravitational waves in the cosmic microwave background (CMB) polarization. It has been shown that a source term assumed to be a correlated Gaussian field with a prescribed Hurst exponent leads to a realistic pattern [24]. Our results on the rand-model provide a possible explanation for the origin of this spatially correlated source term: it would result from the addition of randomly distributed interstellar clouds which radius are actually known to be distributed as a power-law [25].

The rand-model is thus expected to explain the behavior of systems in a variety of contexts ranging from the absorption of light by 2-phase turbulent flows or by aerosols to the microwave emission by interstellar clouds. Further work will extend the results presented here to 2D geometry and obtain quantitative predictions.

ACKNOWLEDGEMENTS

We thank Bernard Legras for discussions related to absorption by aerosols and Francois Boulanger for discussions and for raising our attention to the problem of emission at microwave frequency by interstellar clouds.

APPENDIX

In this appendix, several results presented in the manuscript are described rigorously and justified at a heuristic level. We also provide formula not presented in the article. In particular our aim is to prove that, as the number of random transformations N becomes large, the front h_N and its fluctuations both rescaled with an ad-hoc power of N resembles a typical trajectory of a well identified limiting random process. Deriving these results requires to settle some notations. This is done in subsection A. We present the results for the mean position of the front in subsection B and for the fluctuations in subsection C. We combine a rigorous mathematical presentation with short descriptions adequate for physicists. These descriptions are written in bold letters.

A. Definition

We first need to define the notion of convergence of a random process and in particular the convergence in distribution. To that aim, we denote by C the set of continuous real functions on $[0, D]$, by $||\cdot||_\infty$ the norm of the uniform convergence on $[0, D]$ and by $\mathcal{C}$ the associated Borel σ-algebra. For μ a probability law on $(C, \mathcal{C})$ and for $(X_n)_{n\geq 1}$ a sequence of random continuous functions (defined on a probability space $(\Omega, \mathcal{A}, P)$) we will set

$$X_n \Rightarrow_n \mu \tag{5}$$

when X_n converges in distribution in $(C, \mathcal{C})$ towards μ as $n \to \infty$. By extension if X is a random continuous function, we will set $X_n \Rightarrow_n X$ if X_n converges to the law of X as $n \to \infty$. This convergence can be understood as follows. Consider any bounded continuous functional $g : (C, ||\cdot||_\infty) \mapsto \mathbb{R}$. The latter convergence means that

$$\lim_{n\to\infty} \int_\Omega g(X_n(\omega))dP(\omega) = \int_\Omega g(X(\omega))dP(\omega).$$

This is what mathematicians call convergence in distribution.

Proving rigorously a convergence of type (5) on $(C, \mathcal{C})$ requires the use of mathematical tools from [26, Chapter 2] or [27, Theorem 21.42]. There are two hypotheses to verify to conclude that $X_n \Rightarrow_n X$:

1. the convergence in finite dimensional distributions of X_n towards X. To that aim, for $0 \leq t_1 < t_2 < \cdots < t_k \leq 1$ one has to check that the random vector $(X(t_1), \ldots, X(t_k))$ is the limit in distribution of the sequence $(X_n(t_1), \ldots, X_n(t_k))_{n\geq 1}$. **We note that this is equivalent to the property that the Fourier transform of the vector $(X_n(t_1), \ldots, X_n(t_k))$ converges as $n \to \infty$ towards the Fourier transform of $(X(t_1), \ldots, X(t_k))$.**

2. the tightness of $(X_n)_{n\geq 1}$ in $(C, ||\cdot||_\infty)$ which provides, with a probability arbitrary close to 1, a uniform (in n) control on the modulus of continuity of X_n that is of its fluctuations (in t). This tightness is for instance obtained with the Kolmogorov criterion (stated in [26, Theorem 12.3]) by proving that there exists a $C > 0$ such that for every $0 \leq s < t \leq 1$

$$\sup_{n\geq 1} \int_\Omega |X_n(t, \omega) - X_n(s, \omega)|^2 dP(\omega) \leq C(t - s)^2.$$

Qualitatively, the process must have spatial variations that are not too large (uniformly in the number of iterations).

In summary, if X_n satisfies these two properties, then it converges in distribution towards X.

We also use the well established equality in law between the order statistics of N independent Pareto-distributed random variables of parameter β and the random vector

$$\Big(\Big(\frac{T_{N+1}}{T_1}\Big)^{\frac{1}{\beta-1}},\dots,\Big(\frac{T_{N+1}}{T_N}\Big)^{\frac{1}{\beta-1}}\Big) \tag{6}$$

where $T_0=0$ and $(T_{i+1}-T_i)_{i\geq 0}$ is a sequence of independent and identically distributed (i.i.d.) random variables following an Exponential law of parameter 1. **This, among other properties usefull for physicists, implies that the largest values of N independent Pareto random variables are of order $N^{\frac{1}{\beta-1}}$. We will use this property to justify the behavior at large N of the front as given by eq. 8.**

B. Mean position of the front

Let us be more specific by defining the process h_N. Let $(Z_i)_{i\geq 1}$ be a sequence of independent random variables following a Pareto distribution of parameter $\beta-1$. Then, for the rand-model, we let $(Y_i)_{i\geq 1}$ be an i.i.d. sequence of random variables following a Uniform law on $[0,D]$ whereas for the min-model Y_i is the leftmost point on $[0,D]$ where the minimum of h_{i-1} is attained. Thus, we set for $N\geq 1$

$$h_N(x):=\sum_{i=1}^{N} Z_i^{\alpha-1}1_{[0,Z_i)}(v_{Y_i}(x))\;\psi\Big(\frac{v_{Y_i}(x)}{Z_i}\Big),\;x\in[0,D]. \tag{7}$$

We now present the results for the mean position of the front. In the case $\beta<\alpha$, for both the random and the minimum processes,

$$N^{-\frac{\alpha-1}{\beta-1}}\;h_N\Rightarrow_N R \tag{8}$$

where R is a real random variable, which by abuse of notation is considered here as random function in C that is constant on $[0,D]$. Moreover, R follows a $\frac{\alpha-1}{\beta-1}$ stable-law of characteristic function

$$\Phi(t)=\frac{\beta-1}{2\alpha-\beta-1}\;\exp\Big[\Gamma\big(-\tfrac{\beta-1}{\alpha-1}\big)\,|t|^{-\frac{\beta-1}{\alpha-1}}\;+\;i\,\tfrac{\pi\,(\beta-1)}{2\,(\alpha-1)}\Big]. \tag{9}$$

In the case, $\beta>\alpha$, we obtain

$$N^{-1}\;h_N\Rightarrow_N\;2\,\frac{\beta-1}{D}\;\Big[\int_0^1\psi(u)\,du\int_1^{D/2}z^{\alpha-\beta}dz + \int_{D/2}^{\infty}z^{\alpha-1-\beta}\int_0^{D/2}\psi\big(\frac{y}{z}\big)dydz\Big] \tag{10}$$

that is to say, the limit is a non-random constant function on $[0,D]$.

The critical case $\beta=\alpha$ can also be analyzed rigorously and for both the random and the min model, the following convergence holds true

$$(N\,\log N)^{-1}\;h_N\Rightarrow_N\;1,$$

where, as in the latter case, the convergence takes place towards a non-random constant function that equals 1 on $[0,D]$.

Let us give a heuristic for the growth rate of the front (as a function of N) that becomes ballistic for β larger than α. Recall Eq. (1) of the article and observe that when $\beta>\alpha$, the increments are integrable since $Z^{\alpha-1}$ has a finite first moment. For this reason, the Law of Large Numbers can be applied to the spatial average of both the rand and the min models which equal a sum of independent identically distributed random variables (the integrals of the increments). As a consequence the spatial average of h_N grows linearly in N.

In the case $\alpha>\beta$, we note that $Z^{\alpha-1}$ is a non-integrable heavy-tailed random variable and so are the increments of the front. As a consequence, the law of large number is not applicable anymore. However, the characterization of the order statistics of $(Z_1,\dots,Z_N)$ displayed in (6) allows us to assert that the sum in (7) is dominated by its k largest increments provided k is chosen large enough (but finite and not dependent on N). This explains the convergence in 8 and in particular the super-ballistic rescalling in $N^{\frac{\alpha-1}{\beta-1}}$.

C. Fluctuations

For the rand model, we are able to fully describe the fluctuations of h.

We set $f_N(x)=h_N(x)-h_N(0)$.

1. For $\alpha>1+n$ and $1<\beta\leq\beta_c:=2\alpha-1-2n$

$$N^{-\frac{\alpha-1-n}{\beta-1}}\,f_N^r\Rightarrow_N\mu, \tag{11}$$

where μ is the limiting law on $(C,\mathcal{C})$ of the sequence of continuous processes $(\gamma_N)_{N\in\mathbb{N}}$ defined as

$$\gamma_N(x):=\sum_{i=1}^{N}\frac{G_i(x)}{T_i^{\frac{\alpha-1-n}{\beta-1}}},\quad x\in[0,D], \tag{12}$$

where for $x\in[0,D]$,

$$G_i(x):=\frac{\psi^{(n)}(0)}{n!}\big(v_{Y_i}(x)^n-v_{Y_i}(0)^n\big), \tag{13}$$

where $(Y_i)_{i\in\mathbb{N}}$ is a sequence of i.i.d. random variables following a Uniform law on $[0,D]$. Observe that we used the results of Eq. 6 to obtain Eq. 12. Note also that the convergence of $(\gamma_N)_{N\geq 1}$ occurs

almost surely if $\alpha - 1 - n > \beta - 1$, i.e., $\beta < \alpha - n$. **The interest of this result is that Eq. 11, 12 and 13 provide an explicit formula for calculating or simulating the asymptotic behavior of the front.**

2. For $\alpha \in [1, 1+n]$ or for $\alpha > 1+n$ and $\beta > \beta_c$

$$N^{-\frac{1}{2}} f_N^r \Rightarrow_N Y \tag{14}$$

where Y is a centered Gaussian process with covariance function $r(s,t) = \mathrm{Cov}\,(X_1(s), X_1(t))$. In the case of a triangle ($n = 1$), there exists a $C > 0$ such that

$$r(t,t) := \mathrm{Var}(X_1(t)) \leq C \max\{t^2,\ t^{2\alpha-\beta}\}, \quad t \in [0, D]. \tag{15}$$

For the rand model, the regime change for the growth rate of the fluctuations of the front occurs at β_c because for $\beta > \beta_c$, we enter the domain of application of the Central Limit Theorem. Again, with Eq. (1) of the article, we observe that, since n is the index of the first non zero derivative of ψ at 0, the fluctuations of a single increment $\delta(h(x) - h(0))$ are bounded above and below by a constant time to $Z^{\alpha-1-n}$ which is square integrable for $\beta > \beta_c$ only.

Finally, let us give a short explanation to the fact that when $\beta > \beta_f = 2\alpha - 2$ the covariance $r(s,t)$ has an exponent $2\alpha - \beta > 2$. Let $s < t$. For both s and t to be affected by the transformation it is necessary that $t - s \leq 2Z$. **Moreover $\beta > \beta_f$ implies $\beta > \beta_c$ so that $Z^{\alpha-1-n}$ is square integrable and $E\big[Z^{2(\alpha-1-n)}\, 1_{\{2Z \geq t-s\}}\big]$ behaves as $(t-s)^{2\alpha-\beta}$ which explains our result.**

[1] S. F. Edwards, D. R. Wilkinson, Proc. Roy. Soc. London A 381, 17-31 (1982).
[2] T. Halpin-Healy and Y. C. Zhang, Phys. Reports, 254, 215-415 (1995).
[3] M. Kardar, G. Parisi and Y. C. Zhang, Phys. Rev. Letters 56, 889 (1986).
[4] M. Hairer, Annals of Mathematics, 178 (2), 559–664 (2013).
[5] K. Takeushi, Physica A: Statistical Mechanics and its Applications, 504, 77-105 (2018).
[6] H.K. Janssen, U.C. Täuber and E. Frey, The European Physical Journal B (9), 491–511 (1999).
[7] P. K. Mandal and D. Jana Phys. Rev. E 77, 061604 (2008).
[8] F. L. Forgerini and W. Figueiredo Phys. Rev. E 79, 041602 (2009).
[9] F. Pétrélis, K. Chanard, A. Schubnel, and T. Hatano Phys. Rev. E 107, 034132 (2023).
[10] F. Pétrélis, K. Chanard, A. Schubnel, and T. Hatano, J. Stat. Mech., 043404 (2024).
[11] C.H. Scholz, The Mechanism of Earthquakes and Faulting, Cambridge University Press, 2019.
[12] H. Kanamori and E. E. Brodsky, Reports on Progress in Physics 67(8) 1429 (2004).
[13] H. Kawamura et al., Rev. of modern physics, **84**, 839 (2012)
[14] The magnitudes m of earthquake are distributed as an exponential $\exp -bm$ with b close to unity. m is proportional to $log(S)$ where S is the size of the earthquake so that S is distributed as power-law of exponent close to -2.
[15] F. Renard et al., GRL 40, 83-87 (2013). S. Abe, and H. Deckert, Solid Earth 12, 2407 (2021). L. Bruhat et al., Geophys. J. Intern., 220, 18571877 (2020).
[16] T. Candela et al., Geophysical Journal International, 187, 959-968 (2011).
[17] D. Sornette and Y.-C. Zhang, Geophysical Journal International, 113, 382-386 (1993).
[18] P. Krapivski et al., A Kinetic View of Statistical Physics, Cambridge University Press, Cambridge (2010).
[19] C. Garrett, M. Li, and D. Farmer, Journal of physical oceanography 30, 2163 (2000).
[20] S. Wiederseiner et al., Exp Fluids 50, 1183–1206 (2011).
[21] O. Boucher, Atmospheric Aerosols, Springer Netherlands (2015).
[22] C. Junge, Journal of the atmospheric sciences, 12, 13-25 (1955).
[23] C. White, Journal of Colloid and Interface Science, 87, 204-208 (1982).
[24] Planck collaboration, Astronomy and Astrophysics, 596, A105 (2016).
[25] B.G. Elemegreen and E. Falgarone, Astrophysical Journal, 471, 816-821 (1996).
[26] Billingsley P., Convergence of probability measures, Second. New York: John Wiley & Sons Inc., 1999.
[27] Klenke A., Probability Theory: A Comprehensive Course. Springer, 2007.